Machine GRAPHICS & VISION 7:4 (1998) 807-829

# Linear and Incremental Estimation of Elastic Deformations in Medical Registration Using Prescribed Displacements

Wladimir Peckar[1], Christoph Schnörr[1], Karl Rohr[1],
H. Siegfried Stiehl[1], and Uwe Spetzger[2]

[1]Universität Hamburg, FB Informatik, AB Kognitive Systeme,
Vogt-Kölln-Str. 30, D-22527 Hamburg, Germany
[2]Neurochirurgische Klinik, RWTH Aachen,
Pauwelsstr. 30, D-52057 Aachen, Germany
E-mail: peckar@informatik.uni-hamburg.de

**Abstract**

We propose an approach for estimation of elastic deformations in medical registration. Compared to standard registration methods based on elasticity theory, our estimation scheme does not contain parameters of the deformation model (elastic constants). Rather, the computed elastic deformation is *uniquely* defined through incorporation of prescribed displacements on boundary structures in the source and target image. Under the assumption of correctness of input data, our estimation scheme provides the exact correspondence of structures to be registered due to the constraints. Furthermore, to cope with large-magnitude deformations, we propose an *incremental* model based on successive linearizations of the non-linear elastic equilibrium

equation. To illustrate the performance of our approach, we show experimental results for 2-D and 3-D synthetic as well as real medical images and provide timing information for sequential and parallel realizations.

**Key words**: non-rigid medical image registration, elastic deformations, finite element method.

# 1 Introduction

Comparative analysis of different object representations plays an important role in the clinical routine, since it often helps to improve information required for various applications, like comparison of different tomography modalities for neurosurgery planning. Registration in medical image processing aims at supporting a physician in finding correspondences between image representations of diagnostically or therapeutically relevant objects. It can be formally defined as a mathematical transformation applied to a source image which puts it into spatial correspondence with the target image. Important performance criteria for registration schemes are accuracy, robustness, and time required to compute the transformation. According to the application fields, one can distinguish between three main types of medical registration: single patient registration, image-atlas registration, and inter-patient registration (see, for example, [32] for more details on the classification of registration methods).

Transformations used in medical registration can be divided into rigid and non-rigid as well as into local and global ones [32], where the specific type of transformation to be used depends on the concrete registration task. Local non-rigid transformations are normally used in applications where anatomical variability or metamorphic processes are present and where, as a consequence, rigid transformations may not provide satisfactory registration results. Objects of our interest in this paper will be only local non-rigid transformations.

Several groups of registration methods with local non-rigid transformations are known in the literature. One group is characterized as landmark-

based approaches [5], [26]. Anatomical landmarks are characteristic features, typically points, which have to be found both in the source and target image. They can be manually or (semi-)automatically localized. The obtained correspondences are then used to compute the complete transformation of the source image by using, for example, thin-plate spline (TPS) interpolation [5] or approximation [26]. In [14], a landmark-based approach has been developed, where interpolation with elastic body splines (EBS), derived from elasticity theory, has been used. An important feature of the landmark-based methods is that an analytical expression is available to compute the transformation, and consequently these methods are computationally efficient.

Another group of methods consists of so-called surface-based approaches [22], [30], [31]. These methods first compute a surface match, and the volumetric transformation is then interpolated to agree with this match. In contrast to physically-based methods, the volumetric transformation in surface-based methods is not usually computed to obey physical laws. In [22], [31] for example, a kind of weighted mean interpolation has been used, where the deformation at a point is computed as a weighted linear combination of distortion functions associated with the surfaces.

The approach developed in this paper belongs to physically-based numerical methods [2], [8], where non-rigid transformations are modeled as deformations of physical bodies, such as elastic solids or compressible fluids, driven by applying external forces. Forces are usually derived from image data to minimize some cost function obtained by comparing the source and target image [7], [2]. The image transformations are then computed as numerical solutions of the corresponding material motion equations.

In [7], a linear model based on elasticity theory, which assumed only small deformations, was used to automatically find optimal mappings between CT images and an atlas of brain anatomy. A cross-correlation coefficient between intensity-based properties of local regions in two images was defined to derive forces that drive the elastic deformation of the source image. It has been later improved through the use of a multi-resolution scheme [2], [28] to in-

crease the speed of computations and to avoid local minima. A probabilistic model based on the finite element method, which has been reported to have properties close to the elastic models of [7], [2], has been proposed in [16].

In real applications, however, deformations required for registration are not always limited to locally small deformations. Motivated by this consideration, an approach based on the theory of fluid mechanics has been introduced in [8] and improved in [6] to increase speed. These models exploit the property that fluids do not carry memory about their initial state, thus no increase of the restoring forces happens during the deformation. Hence the fluid models can be applied for computations of large non-linear deformations.

A common limitation of the fluid models in comparison to the elastic approaches mentioned above is that a local intensity-based similarity measure is used for the derivation of forces. This may lead to false matches since intensity properties alone are not always reliable features by measuring similarity between images, e.g. in the case of non-rigid multi-modality registration. In [13], [11] a linear elastic model based not on intensity but shape properties of objects to be registered has been proposed. The elastic deformation is driven by external forces obtained from mapping parametric representations of the outer cortical surface and the boundary of the ventricles in the source and target image. The principal drawbacks of this approach are, however, that it is parameter-dependent and assumes only small deformations.

In this paper, we propose an approach for estimation of elastic deformations in medical registration which exploits, analogously to [13], [11], shape properties of the involved images. Two principal differences are, however, that our approach is parameter-free and is not limited only to small deformations. Input data for our approach are point correspondences (displacements) of boundary structures obtained in a first step of the registration process. This first processing step is not the objective of the present paper. Rather, we focus on the second step of the registration process and develop an approach that incorporates the displacements as hard constraints

into the elastic deformation model. As a consequence, the parameters of the deformation model (elastic constants) are not required in our approach.

In summary, we list several important advantages of our approach which also directly refer to clinical applications as compared to standard physically-based numerical registration methods:

i) We do not use any local intensity-based similarity measure to derive forces which drive the elastic transformation. As a consequence, the images to be registered do not necessarily need to be similar w.r.t. intensity properties, e.g. in the case of non-rigid multi-modality and image-atlas registration.

ii) Driving forces are implicitly used in our approach via incorporating prescribed displacements as constraints. As a consequence, the remaining parameters of the deformation model (elastic constants) drop out from the mathematical formulation of our registration approach, and thus the model does not require careful parameter-tuning to obtain good results. It is important to note that the parameter-free formulation on the one hand limits the degrees of freedom of possible deformations, but on the other hand makes the registration result more predictable.

iii) Since there exists a unique solution to the mathematical problem associated with our registration approach, it can always be guaranteed that the required deformation is obtained and that certain structures in the source image are exactly matched with those of the target image due to the constraints, provided that correct input data are available.

iv) Registration methods based on linearized elasticity theory implicitly assume that only small deformations occur. As this is not always true in real applications, we develop an incremental model to cope with large deformations which are closer to clinical reality.

### Organization of the paper

In Section 2, we present our estimation scheme. We first formulate the solution to the elastic registration problem as a solution of a non-linear equation describing the static equilibrium in elastic materials under applied external

forces. In the following two subsections, we describe two different linearizations of the non-linear equilibrium equation which lead, correspondingly, to our linear and incremental deformation model. We obtain a parameter-free formulation of the deformation models by incorporating a subset of the solution as extra hard constraints (Subsection 2.4). In Subsection 2.5, we describe the discrete implementation of the incremental deformation model, where we distinguish between the models with and without memory. In Subsection 2.6, we introduce criteria which allow us to detect areas of large non-linear deformations in the elastically transformed image in order to determine the application scope of the linear model. In the remainder of the section, we briefly describe the problem of obtaining input data and the numerical implementation of our approach.

Section 3 presents experimental results with our estimation scheme. We performed registration experiments in 2-D (Subsection 3.1) as well as in 3-D (Subsection 3.2). For the 2-D experiment, we give timing results in the uni- and multiprocessor modes.

# 2 Estimation of elastic deformations

## 2.1 General considerations

We first define the notion of elastic registration. Let $\Omega$ be the source image domain. We define an arbitrary transformation $\boldsymbol{\phi} : \Omega \longrightarrow \mathcal{R}^3$ of the source image as:

$$\boldsymbol{\phi}(\boldsymbol{x}) = \boldsymbol{x} + \boldsymbol{u}(\boldsymbol{x}), \tag{1}$$

where $\boldsymbol{u} : \Omega \longrightarrow \mathcal{R}^3$ denotes the displacement field.

We will call *elastic deformation* a smooth, orientation-preserving deformation described by the equations of static equilibrium in elastic materials. In the most general form, assuming that no deformation occurs on the image

boundary, the equilibrium equations can be written in operator form as:

$$\boldsymbol{\mathcal{L}}(\boldsymbol{u}) = \boldsymbol{f}, \tag{2}$$

where $\boldsymbol{\mathcal{L}}$ is the non-linear elasticity operator which we will define later, and $\boldsymbol{f} : \Omega \longrightarrow \mathcal{R}^3$ denotes the external forces.

To solve the registration problem, we usually first need to derive the appropriate external forces by comparing the source and target image and then solve the non-linear equilibrium equation (2) to compute the transformation which will bring the images to be registered into the optimal spatial correspondence. Two possible schemes for linearization of (2) and derivation of input data will be discussed in the following subsections.

We assume that there is no deformation on the boundary of the image domain in our model (homogeneous Dirichlet boundary condition). Hence the non-linear elasticity operator can be written as [10]:

$$\boldsymbol{\mathcal{L}}(\boldsymbol{u}) = -\mathbf{div}\,\{(\boldsymbol{I} + \boldsymbol{\nabla u})\hat{\boldsymbol{S}}\}, \tag{3}$$

where the *second Piola-Kirchhoff* stress tensor $\hat{\boldsymbol{S}} : \bar{\Omega} \longrightarrow \mathcal{M}^3$ is defined as

$$\hat{\boldsymbol{S}} = \lambda\,\mathrm{tr}(\hat{\boldsymbol{E}})\boldsymbol{I} + 2\mu\hat{\boldsymbol{E}}, \tag{4}$$

and

$$\hat{\boldsymbol{E}} = \frac{1}{2}(\boldsymbol{\nabla u}^{\mathrm{T}} + \boldsymbol{\nabla u} + \boldsymbol{\nabla u}^{\mathrm{T}}\boldsymbol{\nabla u}) \tag{5}$$

denotes the *Green-St. Venant* strain tensor. The two positive constants $\lambda$ and $\mu$ are known as the *Lamé* elastic constants.

## 2.2 Linear deformation model

To compute one linear approximation of the elasticity operator, we perform the conventional linearization by using the Fréchet derivative of $\boldsymbol{\mathcal{L}}$:

$$\boldsymbol{\mathcal{L}}(\boldsymbol{u}) = \boldsymbol{\mathcal{L}}(\mathbf{0}) + \boldsymbol{\mathcal{L}}'(\mathbf{0})\boldsymbol{u} + o(\boldsymbol{u}). \tag{6}$$

Since no deformation occurs with the absence of the external forces, we have $\boldsymbol{\mathcal{L}}(\mathbf{0}) = \mathbf{0}$, and by neglecting the last term in (6) we obtain

$$\boldsymbol{f} = \boldsymbol{\mathcal{L}}(\boldsymbol{u}) \approx \boldsymbol{\mathcal{L}}'(\mathbf{0})\boldsymbol{u}. \tag{7}$$

To compute $\boldsymbol{\mathcal{L}}'(\mathbf{0})\boldsymbol{u}$, we simply drop all non-linear terms of $\boldsymbol{\mathcal{L}}(\boldsymbol{u})$ with respect to $\boldsymbol{u}$ and obtain

$$\boldsymbol{\mathcal{L}}'(\mathbf{0})\boldsymbol{u} = -\mathbf{div}\,\boldsymbol{S}, \tag{8}$$

where $\boldsymbol{S} = \lambda\,\mathrm{tr}(\boldsymbol{E})\boldsymbol{I} + 2\mu\boldsymbol{E}$ is the linearized stress tensor and $\boldsymbol{E} = \boldsymbol{\nabla u} + \boldsymbol{\nabla u}^{\mathrm{T}}$ denotes the linearized strain tensor. The linearized equilibrium equation is then given as

$$-\mathbf{div}\,\boldsymbol{S} = \boldsymbol{f}, \tag{9}$$

which is also a compact form of the well-known *Navier* equation [21] that has standardly been used in elastic registration approaches [7], [2], [13].

## 2.3 Incremental deformation model

The principal drawback of the linearization scheme introduced in the previous subsection is that it equivalently describes only small-magnitude deformations, which is not always the case in practical registration tasks. Another possible linearization scheme is the iterative incremental linearization, where applied forces are supposed to vary by small increments, thus causing small deformations in each iteration step. This model is computationally more expensive than the linear model, since a complete linear problem needs to be solved in each step, and from our knowledge has not yet been investigated in elastic registration.

Starting with $n = 0$ and using again the expression for the Fréchet derivative, the incremental linearization scheme can be written as

$$\boldsymbol{\mathcal{L}}(\boldsymbol{u}^{n+1}) = \boldsymbol{\mathcal{L}}(\boldsymbol{u}^{n}) + \boldsymbol{\mathcal{L}}'(\boldsymbol{u}^{n})(\boldsymbol{u}^{n+1} - \boldsymbol{u}^{n}) + o(\boldsymbol{u}^{n+1} - \boldsymbol{u}^{n}), \quad n = 0, 1, \ldots, \tag{10}$$

or by neglecting the last term

$$\boldsymbol{f}^{n+1} - \boldsymbol{f}^{n} = \boldsymbol{\mathcal{L}}(\boldsymbol{u}^{n+1}) - \boldsymbol{\mathcal{L}}(\boldsymbol{u}^{n}) \approx \boldsymbol{\mathcal{L}}'(\boldsymbol{u}^{n})(\boldsymbol{u}^{n+1} - \boldsymbol{u}^{n}), \quad n = 0, 1, \ldots, \quad (11)$$

hence the incremental linearization iteratively approximates the non-linear deformation model by successively solving the corresponding linear problems and is not limited to only small deformations. For the proof of the convergence of the incremental scheme (11), see [10].

## 2.4 Parameter-free estimation of elastic deformations

Since an elastic deformation is only defined when corresponding values have been assigned to the elastic parameters (Lamé's constants), one of the most important problems when using the elastic model is to find optimal values for these parameters. Since no methods for choosing optimal values of the elastic parameters in medical registration have yet been proposed, an important advantage of our approach (described next) is that it does not contain any parameters of the deformation model.

To obtain a parameter-free formulation, we first eliminate one degree of freedom from the elastic model by setting the parameter $\lambda$ to zero. As a consequence, we prevent the lateral shrinking of objects in images when they are stretched. In this case, the solution of the elastic equilibrium equation will be completely controlled by the applied external forces (cf. [2]), since the remaining parameter $\mu$ can be transferred to the right-hand side of the equation and considered as a scaling coefficient for the forces. Another possible advantage of the elimination of the parameter $\lambda$ is that if an object is supposed to grow only in one direction, the driving external forces can be applied only in this direction and no extra forces are needed to prevent object shrinking.

The next important step is to show that this modified equilibrium equation has a unique solution. This means that only one combination of external forces can cause the concrete deformation. For the proof of the uniqueness of the solution in the linear case, we use the variational formulation of the

equilibrium equation (9). It is given as [23]: Find $\boldsymbol{u} \in \boldsymbol{V}$ such that

$$a(\boldsymbol{u}, \boldsymbol{v}) = l(\boldsymbol{v}), \quad \forall \boldsymbol{v} \in \boldsymbol{V}, \tag{12}$$

where the symmetric bilinear form $a(\boldsymbol{u}, \boldsymbol{v})$ and the linear form $l(\boldsymbol{v})$ are defined as:

$$a(\boldsymbol{u}, \boldsymbol{v}) = \int_\Omega \langle \boldsymbol{E}(\boldsymbol{u}), \boldsymbol{E}(\boldsymbol{v}) \rangle \, dx, \tag{13}$$

$$l(\boldsymbol{v}) = \frac{1}{2\mu} \int_\Omega \boldsymbol{f} \cdot \boldsymbol{v} \, dx, \tag{14}$$

and $\boldsymbol{V}$ denotes the space of admissible functions for which the variational problem (12) is well posed. By using the properties of the bilinear ($\boldsymbol{V}$-ellipticity and continuity) and linear (continuity) form in (12), it has been shown that the variational problem (12) has a unique solution, see [23], [10] for details.

Analogously, the variational formulation of our incremental deformation model (11) is given as [23]: Find $\boldsymbol{\delta u}^n \in \boldsymbol{V}$ such that

$$a(\boldsymbol{\delta u}^n, \boldsymbol{v}) = l(\boldsymbol{v}), \quad \forall \boldsymbol{v} \in \boldsymbol{V}, \tag{15}$$

where

$$a(\boldsymbol{\delta u}^n, \boldsymbol{v}) = \int_\Omega \sum_{i,j,p,q=1}^{3} \hat{a}_{ijpq}(\boldsymbol{\nabla u}^n) \partial_p \delta u_q^n \partial_j v_i \, dx, \tag{16}$$

$$l(\boldsymbol{v}) = \frac{1}{\mu} \int_\Omega \boldsymbol{\delta f}^n \cdot \boldsymbol{v} \, dx. \tag{17}$$

In the latter variational formulation, $\boldsymbol{\delta u}^n = \boldsymbol{u}^{n+1} - \boldsymbol{u}^n$, $\boldsymbol{\delta f}^n = \boldsymbol{f}^{n+1} - \boldsymbol{f}^n$ denote correspondingly displacements and forces increments and

$$\hat{a}_{ijpq}(\boldsymbol{\nabla u}^n) = a_{ijpq} + \sum_{k=1}^{3} a_{kjpq} \partial_k u_i^n + \sum_{r=1}^{3} a_{ijrp} \partial_r u_q^n + \\ + \sum_{k,r=1}^{3} a_{kjpr} \partial_r u_q^n \partial_k u_i^n + \sum_{s,r=1}^{3} a_{pjsr} \hat{E}_{sr}(\boldsymbol{u}^n) \delta_{iq},$$

where $a_{ijpq} = \frac{1}{2}(\delta_{ip}\delta_{jq} + \delta_{iq}\delta_{jp})$, $i, j, p, q = 1, 2, 3$, and $\delta_{ij}$ is Kronecker's symbol.

An important advantage of the variational formulation is that its discrete representation is readily obtained by applying the finite element method (FEM). For discretization of (12) and (15), we used the *Galerkin* method [9]. For details on the FEM discretization of the equilibrium equations, see [23].

By using the uniqueness of the solution of the equilibrium equation, we can *implicitly* define the required external forces, by incorporating a subset of solution as extra constraints in the discrete representations of the equation with the absence of the explicit external forces on its right-hand side. As a consequence, the remaining elastic parameter $\mu$ drops out from our formulation, thus making it completely parameter-free. Incorporation of prescribed displacements in our model requires a modification of the matrix and of the right-hand side vector of the linear equation system corresponding to the discrete representation of the deformation model. It can be shown, that this modification of the linear systems corresponding to (12) and (15), respectively, preserve symmetry and positive definiteness [23]. As a result, we obtain as unique solution a displacement field which exactly fits given local correspondence input data, without the need to specify external forces in an ad-hoc manner.

## 2.5 Discrete implementation of the incremental model

When implementing the incremental model on a discrete grid, the deformation gradient is approaching zero after some iterations due to discretization (cf. [8]). As a consequence, the matrix associated with the discrete incremental model becomes badly conditioned and its update required in each step of the iterative procedure cannot be performed.

One possibility to obviate this problem is to stop the updates of the matrix if the value of the deformation gradient falls below some selected threshold and to use this discrete approximation of $\boldsymbol{\mathcal{L}}'(\boldsymbol{u}^n)$ in the following iteration steps. In this case, we will preserve memory about several preceding

iterations in our model. Formally, we can write:

$$\boldsymbol{\mathcal{L}'}(\boldsymbol{u}^n) \approx \boldsymbol{\mathcal{L}'}(\boldsymbol{u}^k), \quad k = \max\{i \in \{0, \ldots, n\} \,|\, \det(\boldsymbol{I} + \boldsymbol{\nabla u}^i) \geq \epsilon\}. \tag{18}$$

Another possibility is to use $\boldsymbol{\mathcal{L}'}(\boldsymbol{0})$ as an approximation of $\boldsymbol{\mathcal{L}'}(\boldsymbol{u}^n)$ in the iteration process. This latter method is analogous to the *chord* method for iteratively solving non-linear systems of equations [20]. In this case, no memory about preceding deformations is preserved. Such a behavior is analogous to the one of fluids where the restoring forces can relax over time [8].

The difference between the two incremental models can be seen in Figure 1, where we also compared the two formulations of the incremental model (11) with the linear elastic model (7). We prescribed large displacements in the middle of a 25x25 rectangular grid (top row/left). The deformation computed with the linear model is shown in the right image of the top row of the figure. One can see that a topology violation occurred, since the linear model is not suitable for computations of large deformations. In the bottom row of Figure 1, the deformations computed due to the incremental model with and without memory are shown. The value of $\epsilon$ in (18) was chosen to be 0.2. One can see that the deformation without memory (right image) is more smooth than the deformation where memory about some previous iterations was preserved (left image). However, both incremental deformations preserved the topology of the grid.

## 2.6 Criteria for large deformations

As we have already mentioned, the derived linear registration model may cause topology violations in applications where computations of large deformations are needed. Since the linear model is computationally more efficient than the incremental one, a very important problem in registration is to decide which deformations can be considered to be large. In other words, a reliable criterion is needed to determine which kinds of deformations are beyond the scope of the linear model. It has also been reported for other

linear approaches based on elasticity theory that they are not suitable for computations of large deformations [7], [2], [11], but no criteria have been given, which registration problems are out of the application scope of the linear models. However, such investigation has been done in [4] for the TPS model of Bookstein [5], where a general criterion based on a definition of small strain has been applied.

There exists the following formal definition of small strain [21]: Strain can be considered to be small if all components of the displacement gradient $\boldsymbol{\nabla u}$ are small compared to unity.

One can also see that if this condition is satisfied, the Green-St. Venant strain tensor can be approximated as

$$\hat{\boldsymbol{E}}(\boldsymbol{u}) = \frac{1}{2}\left(\boldsymbol{\nabla u}^{\mathrm{T}} + \boldsymbol{\nabla u} + \boldsymbol{\nabla u}^{\mathrm{T}}\boldsymbol{\nabla u}\right) \approx \frac{1}{2}\left(\boldsymbol{\nabla u}^{\mathrm{T}} + \boldsymbol{\nabla u}\right) = \boldsymbol{E}(\boldsymbol{u}). \tag{19}$$

By using the latter consideration, we define a deformation to be large if there exists a component of the displacement gradient which is greater than some $\xi \ll 1$. In addition, we can determine areas after elastic deformation where the linear approximation of the Green-St. Venant strain tensor was not satisfactory by comparing its linear and non-linear terms.

Formally, our criteria can be written: The linear strain approximation for large deformations is satisfactory if (we consider for simplicity the 2-D case):

$$|\partial_1 u_1| \gg \frac{1}{2}|(\partial_1 u_1)^2 + (\partial_1 u_2)^2| \quad \text{and} \quad |\partial_1 u_1| > \xi, \tag{20}$$

$$|\partial_2 u_2| \gg \frac{1}{2}|(\partial_2 u_1)^2 + (\partial_2 u_2)^2| \quad \text{and} \quad |\partial_2 u_2| > \xi, \tag{21}$$

$$|\partial_2 u_1 + \partial_1 u_2| \gg |\partial_1 u_1 \partial_2 u_1 + \partial_1 u_2 \partial_2 u_2| \quad \text{and} \quad |\partial_2 u_1| > \xi \quad \text{or} \quad |\partial_1 u_2| > \xi. \tag{22}$$

The comparison of the linear and non-linear terms of the Green-St. Venant strain tensor in (20)-(22) has also been used as a criterion in [4] for the TPS model. In this work, we additionally require $|\partial_i u_j| > \xi,\ i, j = 1, 2, 3$ in order to distinguish between small and large deformations. We have applied these criteria to a 2-D registration experiment described in Section 3 to detect large non-linear deformation areas (see Figure 4).

The criteria (20)-(22) allow us to determine the large deformation areas only after having computed the elastic transformation. One can also mention the criterion used by Christensen et al. [8], where a comparison of the determinant of the deformation gradient with a threshold value after each iteration step was carried out to avoid topology violations when applying the fluid registration approach. It is, however, desirable to have a criterion for the input data which could help us to predict undesirable effects, e.g. topology violations, before applying the elastic transformation. This point is the objective of current research.

## 2.7 Prescribed displacements as input data

As input data, our elastic deformation model requires a subset of the solution. Analogously to [13], [11], we use for this purpose displacements on object boundaries, assuming that they can be found both in the source and the target image. Examples for such boundary structures, for example in tomographic brain images, are the outer brain contour and the boundary of the ventricular system. Compared to intensity-based methods for the derivation of input data [7], [2], [8], an important advantage of using boundary mapping is that we use shape properties of images, which are generally robust and modality invariant features compared to intensity properties.

The input correspondences of boundary structures can be obtained by using, for example, active surface models [12], [27], or alternatively by applying boundary matching algorithms such as, for example, curvature-based methods [1], [18]. In this paper, however, we do not attempt to discuss in detail the concrete methods which could be applied for definition of the required boundary mapping.

## 2.8 Numerical solution

After discretization, we obtain the displacement field for deformation from a system of linear equations. Due to the properties of the bilinear form in

the variational formulations of the elastic equilibrium equations (7), (11), the matrix of the system is sparse, symmetric, and positive definite [23]. As a consequence, we can use efficient Krylov-subspace methods [17] to iteratively solve our system of equations. For our experiments, we used the method of conjugate gradients (CG) which is known as probably the most efficient solving method for large linear equation systems with sparse symmetric positive definite matrices typically arising from FEM applications [29]. To reduce memory requirements for matrix storage, we used a special compact band storage scheme [29].

To reduce the condition number of the matrix in the system and consequently to reduce the number of iterations required to solve the system, the optimal preconditioning is very important. To test the performance of our solver, we have applied the CG-method without any preconditioning and in combination with the *Jacobi* and *block Jabobi* preconditioners as well as *incomplete Cholesky factorization* (ICC) [29]. The results are given in Table 1.

# 3 Experiments

In this section, we present some experimental results obtained with our elastic deformation model.

## 3.1 2-D registration experiment

In our first experiment, we registered pre- and post-operative $256 \times 256$ 2-D MR images of the same patient using our linear model. These images are depicted in the top row of Figure 2. Prior to elastic registration, the two 3-D data sets were globally registered by using an affine transformation. For computation of this transformation, we used 5 pairs of landmarks which were manually localized. As corresponding structures for elastic transformation, we took the outer and the inner skin contours which were extracted by using an edge detector. Additionally, we used the brain surface contours, the contours of the right lateral ventricle, and the contour of the tumor in the

source image together with the contour of the resection area in the target image which were manually as well as semi-automatically (using a snake approach [19]) determined. They are depicted in the bottom row of Figure 2. Additionally, we fixed two boundary structures in the source image: the occipital part of the midline of the brain and a part of the dura mater in the brain shift area at the top of the brain. The input data for elastic transformation were obtained through the use of the minimal distance algorithm [3] (for the skin contours) and from the snake model for all other structures (see [24] for more details about obtaining correspondences using the snake model). The result of elastic registration is shown in Figure 3. One can see that a more accurate match of the corresponding anatomical structures has been achieved after elastic registration (bottom image) compared to global affine registration (top image). Local elastic transformation has also allowed to cope with metamorphic processes due to the tumor resection. Another approach to cope with deformations due to brain shifts, which is based on a three component tissue model, has been proposed in [15].

By observing the deformed image in Figure 3/bottom, we can conclude that the most considerable deformations occurred in the areas of the tumor, the brain shift, and the skin in the operation area. We then used the criteria (20)-(22) to detect large non-linear deformations during the experiment. The value of the threshold $\xi$ was chosen to be 0.2. The results are shown in Figure 4. These results correspond quite well with the expectations which can be made by visually observing the elastically deformed image.

Since the assumption of only small deformations is obviously not satisfied for this experiment, we have repeated it using 10 iteration steps of our incremental model. For comparison, we show the enlarged tumor areas in the images deformed with the linear model and incremental model with and without memory in the left row of Figure 5. In the right row, grid deformations for the same areas are shown where one can see that the incremental model without memory showed the best results.

For this experiment, we have also tested the performance of our iterative

linear solver based on the method of conjugate gradients. For this purpose, we used PETSc (the Portable, Extensible Toolkit for Scientific Computation) software package [25]. We first tested how the preconditioning influences the number of iterations and the computation time. For discretization of the image plane, we used a very simple adaptive scheme, where fine discretization is performed only within the common bounding box of the source and target image. The results are presented in Table 1. All the results are given for one processor of a multi-processor SGI Power Challenge computer. Only the time required to solve the linear system is given, the matrix compilation and incorporation of constraints require some extra time. One can see that the preconditioning substantially reduces the iteration steps and, consequently, the computation time.

Next, we tested the effects of parallelization on the computation time. We used for this purpose an SGI Power Challenge computer and parallelization tools provided by PETSc. All computations have been done using the block Jacobi preconditioning. The results are given in Table 2. One can see that an approximately double decrease of the computation time can be achieved by a double increase of the number of processors used. The dependence of the computation time on the number of processors is shown in Figure 8.

## 3.2 3-D registration experiment

In our second experiment, we linearly and incrementally registered a 3-D synthetic image with a part of the cortical surface from a real image. The boundary of the cube was matched to the cortical boundary by using the 3-D minimal distance algorithm. The size of both images was $80 \times 80 \times 80$ voxels. The computation of elastic deformation took about 23 minutes on a single processor of an SGI Power Challenge. The result of the experiment using the linear model is presented Figure 6. One can see that despite the complicated shape of the cortical surface, a rather good approximation of it was obtained (top row). In the middle row of Figure 6, magnitudes of the displacement field are shown for the slices 15, 30, 45. In the bottom row of the figure,

the deformations of the slices 15, 30, 45 are represented as deformations of a rectangular regular grid.

For some slices, however, the application of the linear model caused topology violations, as it is shown for slice 60 in the top row of Figure 7. For comparison, the deformation computed with 10 iteration steps of the incremental model without memory for the same slice is shown in the bottom row of the figure. One can see that the incremental model provided much better results compared to the linear model.

# 4 Discussion

In this paper, we have described a linear and an incremental approach for estimation of elastic deformations in medical registration. Compared to other physically-based numerical methods, our approach does not contain the parameters of the deformation model (elastic constants). The computed elastic deformation is solely constrained through incorporation of prescribed displacements obtained by mapping boundary structures in the source and target image. Our incremental deformation model circumvents the principal drawback of the models based on linear elasticity theory which assume only small deformations. We have also described criteria for detecting areas of large non-linear deformations in the transformed image.

From the experimental results, we could see that the linear model caused in some cases topology violations when deforming grids in contrast to the incremental models. From the described two incremental models, the model without memory showed somewhat better results. This model is analogous to the fluid model [8], where no memory about the undeformed state is preserved, thus more smooth deformations are obtained.

Probably one of the most important points concerning the usage of our deformation model in practical applications which we currently investigate is the problem of obtaining accurate correspondences between boundary structures in the source and target image. In this paper, we used for demonstration

purposes the snake model and the minimal distance algorithm. Their usage in real applications is, however, limited due to the complexity of medical data. Our elastic deformation model does not contain any parameters to influence the reliability of the input data, thus the development of robust methods for definition of the input boundary mapping is needed.

Another important research subject is the efficient numerical implementation of our approach. The implemented method of conjugate gradients with preconditioning shows acceptable results (several seconds in 2-D or minutes in 3-D in the sequential realization) if the matrix can completely be loaded into the computer memory. However, this is not always possible in the 3-D case due to the large number of variables of the deformation model. One possibility to obviate this problem is to use highly adaptive grids for FEM discretization of image domains. This can substantially reduce the number of nodal points and, consequently, the variables of our model. Another point in the numerical implementation is the detailed investigation of the use of parallel and multi-grid solvers which can considerably accelerate our approach. As an example, we showed that the double increase of the number of processors used results in approximately double decrease of the computation time required to register pre- and post-operative 2-D medical images.

Although our approach is physically-based, it is important to note that the developed registration model can only be considered an approximation of a realistic model of deformation processes in biological materials. Only a subset of such materials can be considered as an elastic medium. Moreover, only one elastic parameter is implicitly present in our model as a scaling factor for the applied forces. Also, the injectivity condition, which is necessary for any physical deformation, may not be satisfied in our model due to discretization. As a result, the non-rigid transformations obtained on the basis of our registration model do not exactly correspond to real physical deformations. The development of realistic models of biological materials is a very challenging problem, which is nowadays a subject of intensive research. Besides registration, surgery planning and education are further possible application

areas of models of real biological materials.

### Acknowledgments

Medical image data were kindly provided by the Neurosurgical Clinic (Director: Prof. Dr. J.-M. Gilsbach), University Hospital Aachen of the RWTH.

# A Notation

| | |
|---|---|
| $\mathcal{R}$ | space of real numbers |
| $\mathcal{M}^n$ | space of real square matrices of order $n$ |
| $\boldsymbol{e}_1, \boldsymbol{e}_2, \ldots, \boldsymbol{e}_n$ | basis vectors in $\mathcal{R}^n$ |
| $\Omega$ | bounded open subset of $\mathcal{R}^n$ |
| $\bar{\Omega}$ | closure of the set $\Omega$ |
| $\partial_i = \partial/\partial x_i$ | partial derivative with respect to $x_i$ |
| $\partial^\alpha$ | partial derivative of order $\alpha$ |
| $\boldsymbol{u} \cdot \boldsymbol{v} = \boldsymbol{u}^{\mathrm{T}}\boldsymbol{v}$ | vector inner product |
| $\det(\boldsymbol{A})$ | determinant of a matrix |
| $\mathrm{tr}(\boldsymbol{A}) = \sum_i a_{ii}$ | trace of a matrix |
| $\langle \boldsymbol{A}, \boldsymbol{B} \rangle = \mathrm{tr}(\boldsymbol{A}^{\mathrm{T}}\boldsymbol{B})$ | usual matrix inner product |
| $\mathbf{div}\, \boldsymbol{T} = \sum_i \sum_j \partial_j T_{ij} \boldsymbol{e}_i$ | divergence of a tensor field |

# References

[1] A.A. Amini, R.L. Owen, P. Anandan, and J.S. Duncan. Non-rigid motion models for tracking the left-ventricular wall. In *Lecture Note in Computer Science: Information Processing in Medical Images*, pages 343–356. Springer-Verlag, 1991.

[2] R. Bajcsy and S. Kovačič. Multiresolution elastic matching. *Computer Vision, Graphics, and Image Processing*, 46:1–21, 1989.

[3] P.J. Besl and N.D. McKay. A method for registration of 3-D shapes. *IEEE Transactions on Pattern Analysis and Machine Intelligence*, 14(2):239–256, 1992.

[4] L. Binder, K. Rohr, R. Sprengel, and H.S. Stiehl. Bildregistrierung mit interpolierenden "Thin-Plate Splines" und Bezüge zur linearen Elastizitätstheorie. In *Proc. of 18. DAGM-Symposium Mustererkennung*, pages 281–288, Heidelberg, September 1996. Springer-Verlag.

[5] F.L. Bookstein. Principal warps: Thin-plate splines and the decomposition of deformations. *IEEE Transactions on Pattern Analysis and Machine Intelligence*, 11(6):567–585, 1989.

[6] M. Bro-Nielsen and C. Gramkow. Fast fluid registration of medical images. In *Proc. Visualization in Biomedical Computing (VBC'96)*, volume 1131 of *Lecture Notes in Computer Science*, pages 267–276, Hamburg, Germany, September 1996. Springer-Verlag.

[7] C. Broit. *Optimal Registration of Deformed Images*. Doctoral dissertation, University of Pennsylvania, August 1981.

[8] G.E. Christensen, R.D. Rabbitt, and M.I. Miller. Deformable templates using large deformation kinematics. *IEEE Transactions on Image Processing*, 5(10):1435–1447, 1996.

[9] P.G. Ciarlet. *The Finite Element Method for Elliptic Problems*, volume 4 of *Studies in Mathematics and its Applications*. North-Holland, Amsterdam, 1978.

[10] P.G. Ciarlet. *Mathematical Elasticity. Volume I: Three-Dimensional Elasticity*, volume 20 of *Studies in Mathematics and its Applications*. North-Holland, Amsterdam, 1988.

[11] C. Davatzikos. Spatial transformation and registration of brain images using elastically deformable models. *Computer Vision and Image Understanding, Special Issue on Medical Imaging*, 66(2):207–222, 1997.

[12] C. Davatzikos and R.N. Bryan. Using a deformable model to obtain a shape representation of the cortex. *IEEE Transactions on Medical Imaging*, 15:785–795, 1996.

[13] C. Davatzikos, J.L. Prince, and R.N. Bryan. Image registration based on boundary mapping. *IEEE Transactions on Medical Imaging*, 15(1):112–115, 1996.

[14] M.H. Davis, A. Khotanzad, D.P. Flaming, and S.E. Harms. A physics-based coordinate transform for 3-D image matching. *IEEE Transactions on Medical Imaging*, 16(3):317–328, June 1997.

[15] P.J. Edwards, D.L.G. Hill, J.A. Little, and Hawkes. D.J. Deformation for image guided interventions using a three component tissue model. In J. Duncan and G. Gindi, editors, *Proc. 15th Internat. Conf. Information Processing in Medical Imaging (IPMI'97)*, pages 218–231, Poultney, Vermont, USA, June 1997. Springer-Verlag.

[16] J.C. Gee, D.R. Haynor, M. Reivich, and R. Bajcsy. Finite element approach to warping brain images. In *Proc. SPIE Image Processing*, volume 2167, pages 327–337, 1994.

[17] W. Hackbusch. *Iterative Solution of Large Sparse Systems of Equations.* Springer-Verlag, 1993.

[18] C. Kambhamettu and D. Goldgof. Curvature-based approach to point correspondence recovery in conformal non-rigid motion. *CVGIP: Image Understanding*, 60(1):26–43, 1994.

[19] M. Kass, A. Witkin, and D. Terzopoulos. Snakes: Active contour models. *International Journal of Computer Vision*, 1(4):321–331, 1988.

[20] C.T. Kelley. *Iterative Methods for Linear and Nonlinear Equations.* SIAM, Philadelphia, 1995.

[21] L.E. Malvern. *Introduction to the Mechanics of a Continuous Medium.* Prentice-Hall, 1969.

[22] M. Moshfeghi, S. Raganath, and K. Nawyn. 3-D elastic matching of volumes. *IEEE Transactions on Image Processing*, 3(2):128–138, 1994.

[23] W. Peckar. *Application of Variational Methods to Elastic Registration of Medical Images.* Doctoral dissertation, Logos-Verlag, Berlin, 1998.

[24] W. Peckar, C. Schnörr, K. Rohr, and H.S. Stiehl. Two-step parameter-free elastic image registration with prescribed point displacements. In *Proc. 9th Int. Conf. on Image Analysis and Processing (ICIAP '97)*, volume 1310 of *Lecture Notes in Computer Science*, pages 527–534, Florence, Italy, September 1997. Springer-Verlag.

[25] PETSc World Wide Web page. http://www.mcs.anl.gov/Projects/petsc/petsc.html, November 1997.

[26] K. Rohr, H.S. Stiehl, R. Sprengel, W. Beil, T.M. Buzug, J. Weese, and M.H. Kuhn. Point-based elastic registration of medical image data using approximating thin-plate splines. In *Proc. Visualization in Biomedical Computing (VBC'96)*, volume 1131 of *Lecture Notes in Computer Science*, pages 297–306, Hamburg, Germany, September 1996. Springer-Verlag.

[27] S. Sandor and R. Leahy. Surface-based labeling of cortical anatomy using a deformable atlas. *IEEE Transactions on Medical Imaging*, 16(1):41–54, 1997.

[28] T. Schormann, S. Henn, and K. Zilles. A new approach to fast elastic alignment with applications to human brains. In *Proc. Visualization in Biomedical Computing (VBC'96)*, volume 1131 of *Lecture Notes in Computer Science*, pages 337–342, Hamburg, Germany, September 1996. Springer-Verlag.

[29] H.R. Schwarz. *Methode der finiten Elemente.* Teubner, Stuttgart, 1984.

[30] R. Szeliski and S. Lavallée. Matching 3-D anatomical surfaces with non-rigid deformations using octree-splines. *International Journal of Computer Vision*, 18(2):171–186, 1996.

[31] P. Thompson and A. Toga. A surface-based technique for warping three-dimensional images of the brain. *IEEE Transactions on Medical Imaging*, 15(4):401–417, 1996.

[32] P.A. van den Elsen, E.-J.D. Pol, and M.A. Viergiever. Medical image matching: A review with classification. *IEEE Engineering in Medicine and Biology Magazine*, 12(1):26–39, 1993.

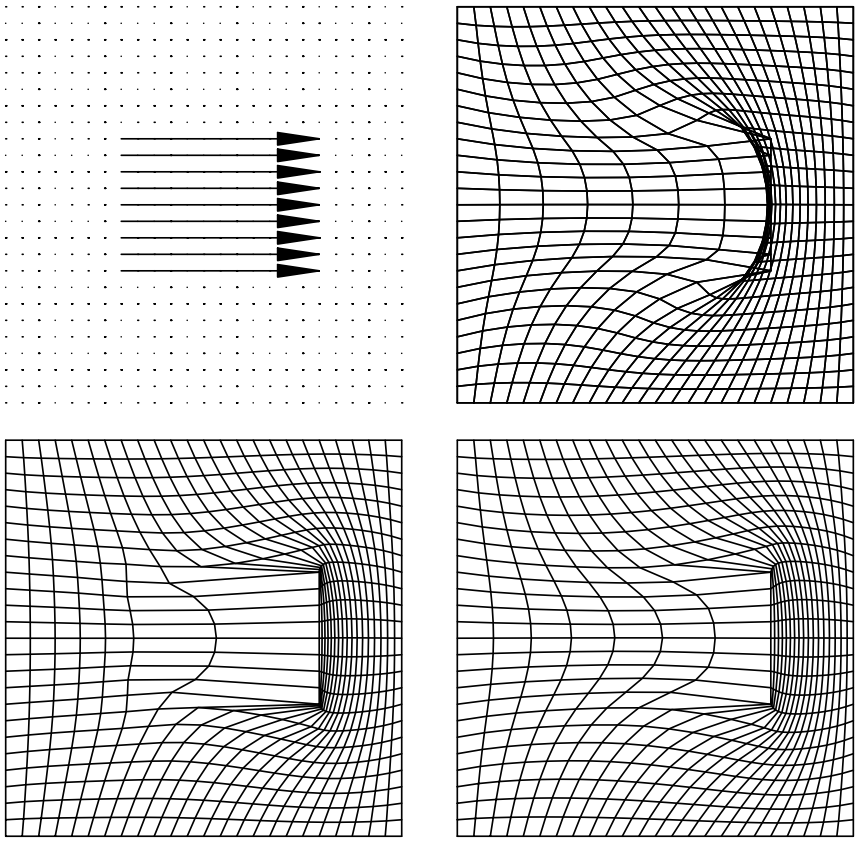

Figure 1: Deformation with large displacements. Top row/left: Prescribed displacements. Top row/right: Deformation computed with the linear model. Bottom row: Deformation computed with the incremental model with memory (left) and without memory (right). One can see that the incremental model preserves the topology when computing large deformations.

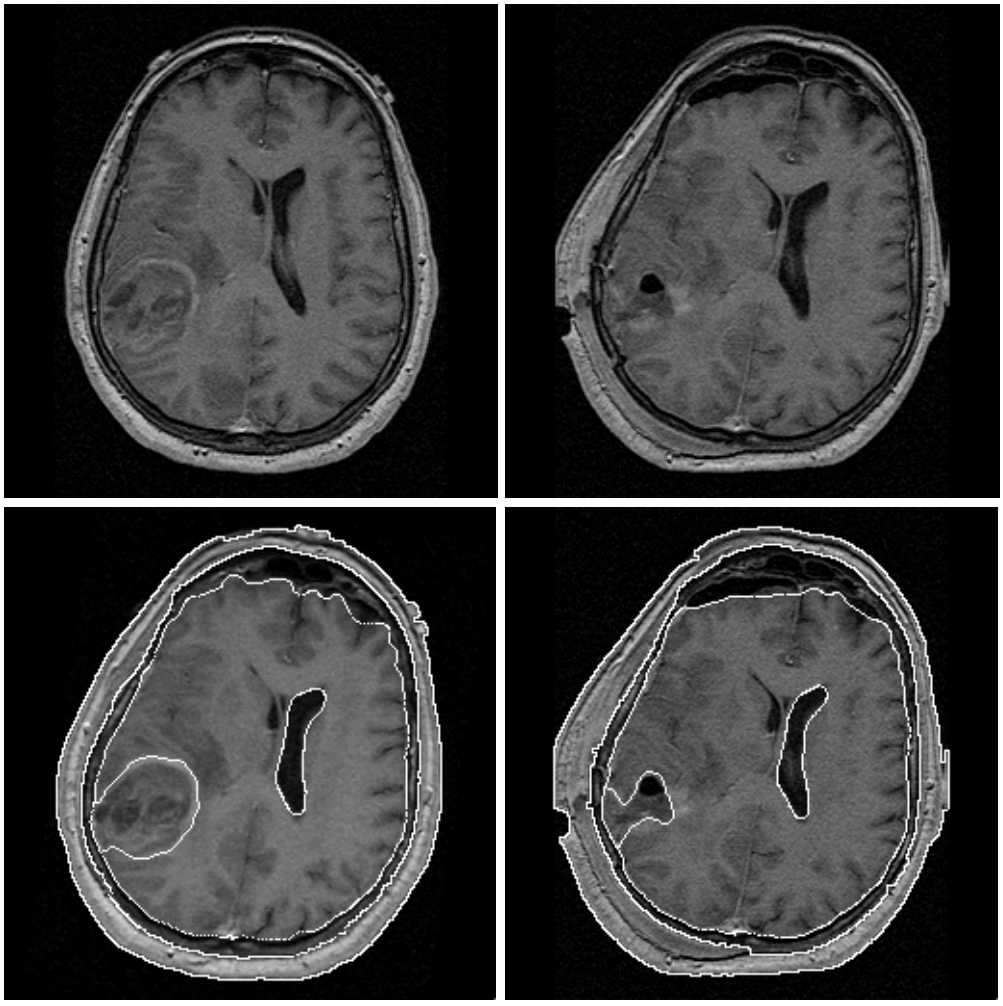

Figure 2: 2-D registration example using the linear model. Top row: Two MR slices taken from the same patient with the pre-operative source image at the left. Bottom row: Corresponding structures, as determined by a clinical expert, in the globally transformed source image and in the target image.

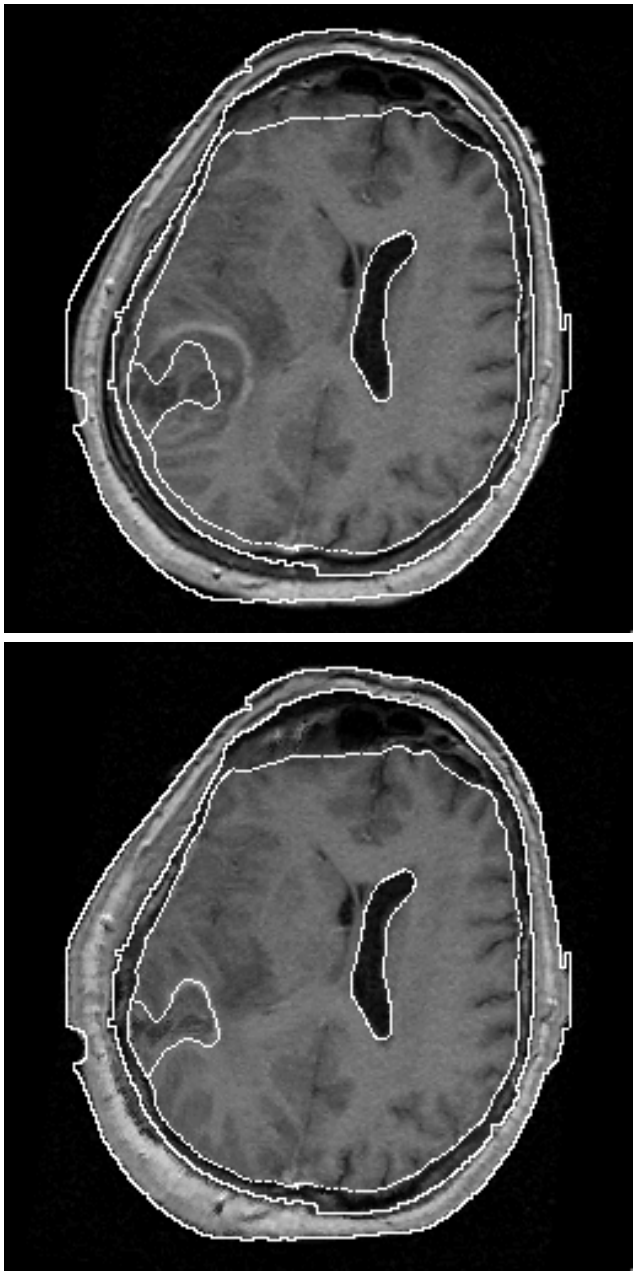

Figure 3: 2-D registration example using the linear model. Top image: Result of affine registration. Bottom image: Result of elastic registration. More accurate registration of the corresponding structures was obtained in comparison to the global transformation. Additionally, the elastic transformation coped with the metamorphic processes (tumor resection and brain shift).

Figure 4: Large non-linear deformation areas for the 2-D registration example in Figures 2-3. Top: Expansion in $x$-direction. Middle: Expansion in $y$-direction. Bottom: Pure shear. As one can see, the assumption of only small deformations is not satisfied for the experiment.

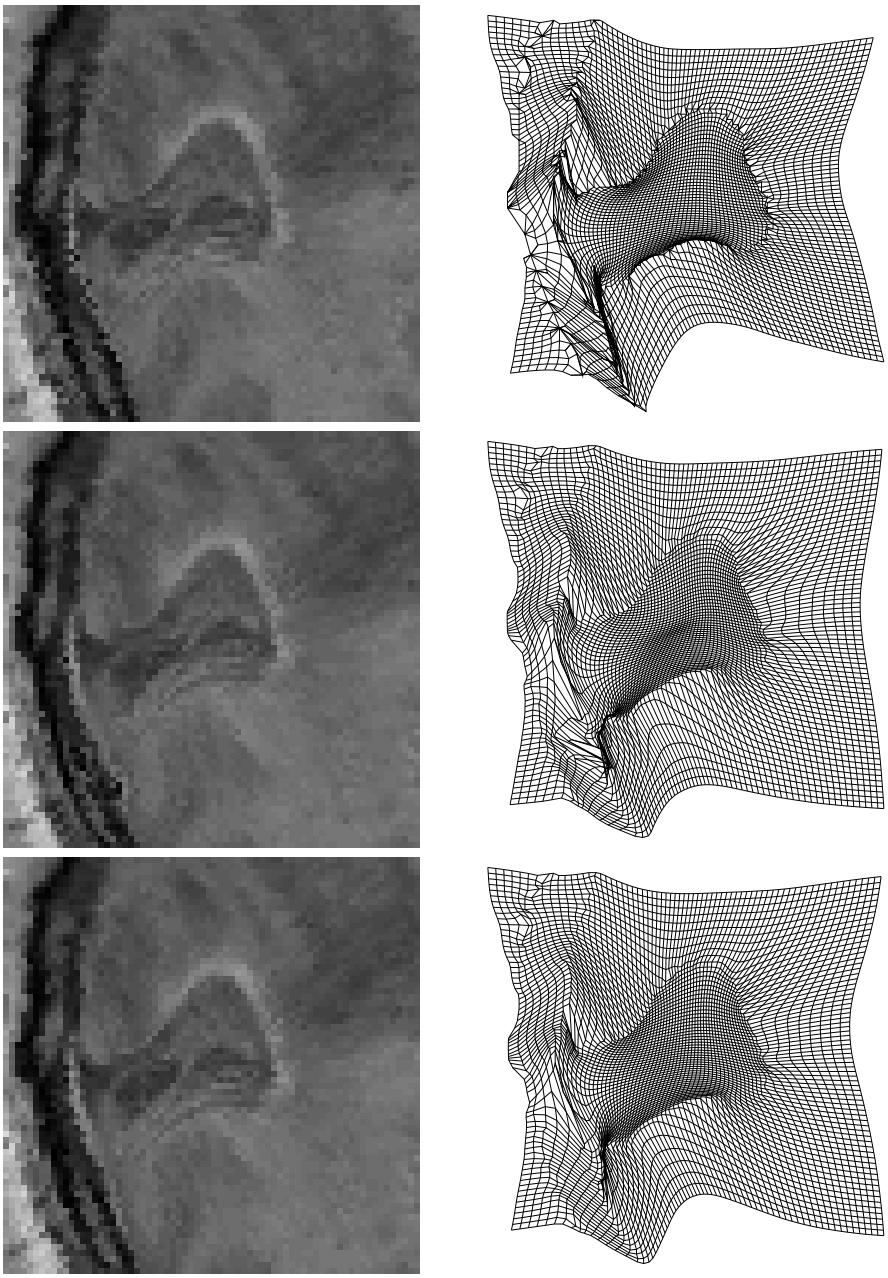

Figure 5: Comparison between elastic deformation models for the 2-D registration example in Figure 2. Top row: Linear model. Middle row: Incremental model with memory. Bottom row: Incremental model without memory.

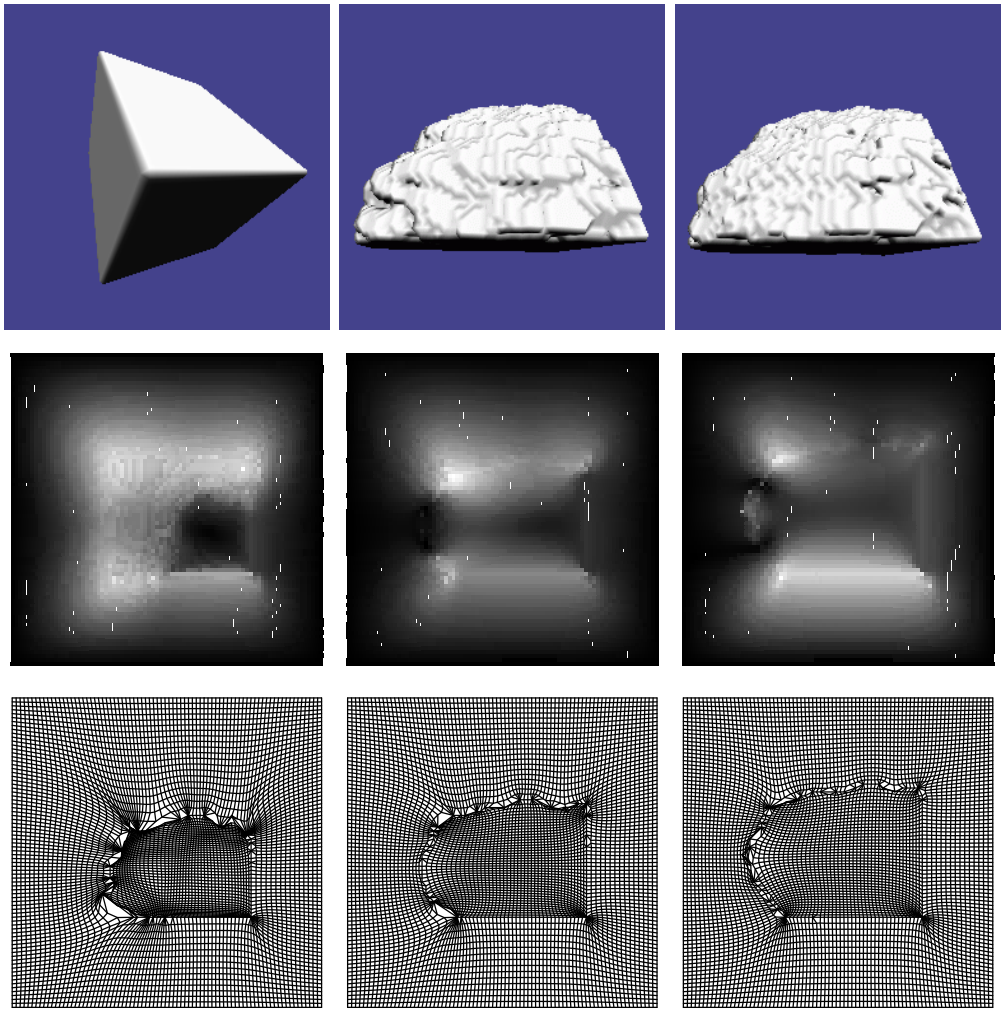

Figure 6: 3-D registration experiment. Top row: Source, target, and deformed source image. Middle row: Magnitudes of the displacement field for the horizontal slices 15, 30, 45. Bottom row: Deformations of the horizontal slices 15, 30, 45 projected onto the $xy$-plane.

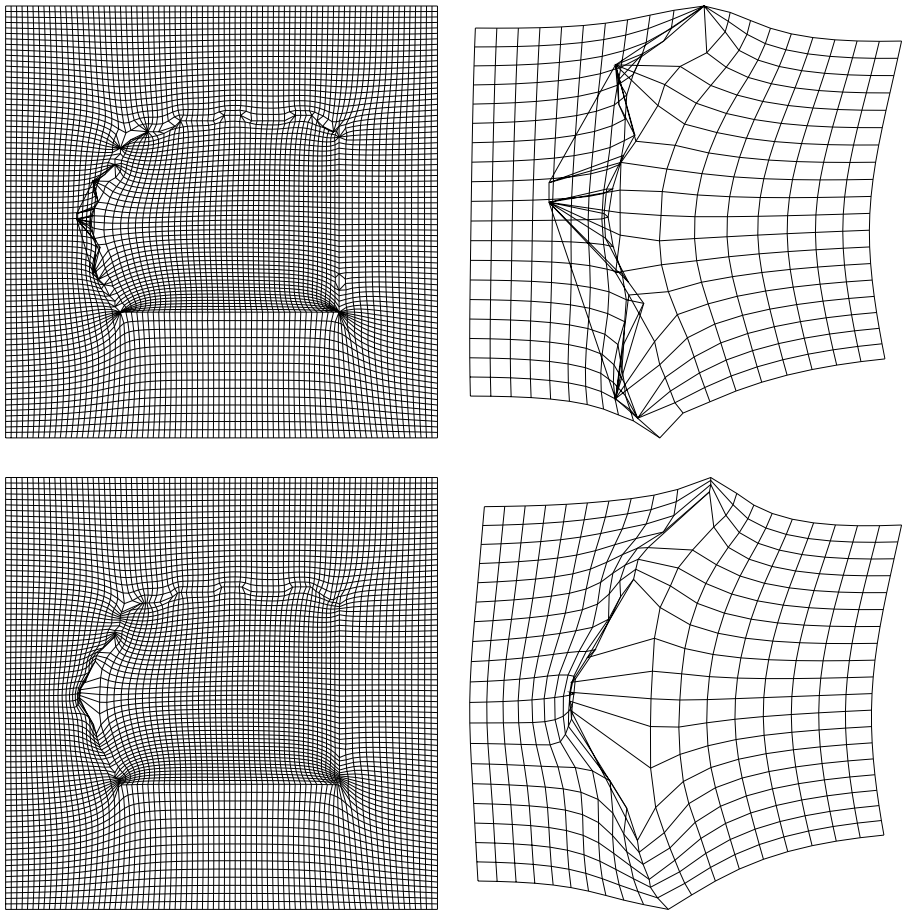

Figure 7: Comparison of the linear and incremental model for the 3-D registration experiment in Figure 6. Top row: Slice 60 of the 3-D image deformed using the linear model and its enlarged section. Bottom row: The same slice of the image deformed using the incremental model without memory and its enlarged section. One can see that the incremental model does not suffer from considerable violation of the grid topology, as in the case with the linear model.

| | Number of iterations | Time (sec.) |
|---|---|---|
| No preconditioning | 628 | 187.5 |
| Jacobi | 215 | 66.9 |
| Block Jacobi | 54 | 41.7 |
| ICC | 54 | 39.9 |

Table 1: 2-D registration: Timings for the uniprocessor mode.

| Number of processors | 1 | 2 | 4 | 8 | 16 |
|---|---|---|---|---|---|
| Number of iterations | 54 | 60 | 66 | 69 | 76 |
| Time (sec.) | 41.7 | 20.6 | 11.0 | 4.4 | 2.1 |

Table 2: 2-D registration: Timings for the multiprocessor mode.

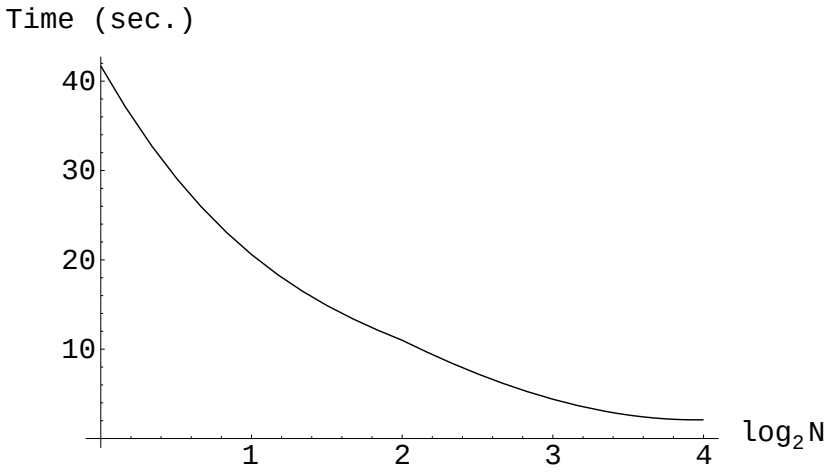


Figure 8: Dependence of the computation time on the processors number $N$.